Ceramics International **22** (1996) 7–14

0272-8842(95)00025-9
0272-8842/96/$15 00

Pore Structure Evolution During Solvent Extraction and Wicking

Sang Woo Kim,[a] Hae-Weon Lee,[b] Huesup Song[b] & Byung Ho Kim[a]

[a]Department of Materials Science and Engineering, Korea University, Seoul 136–701, Korea
[b]Division of Ceramics, Korea Institute of Science and Technology, P.O. Box 131 Cheongryang, Seoul, Korea

(Received 3 January 1995; accepted 6 February 1995)

Abstract: Pore structure evolution and binder distribution during both solvent extraction and wicking were investigated for plastic-formed ceramic bodies. The solvent extraction rate had a $t^{1/2}$ dependence, while the wicking rate varied depending on the degree of saturation. There existed a debinding front separating the debinded region (with pendular state) from the undebinded region (with fluid state) during solvent extraction, while the green body went through sequential transitions of capillary structure as a whole during wicking with the help of the rapid re-distribution of the binder system. In fact, the debinding process by wicking could be divided into four regimes: (i) the rapidly falling rate regime up to capillary state, (ii) a constant rate regime up to the funicular state, (iii) the first slowly falling rate regime to the pendular state, and (iv) the second slowly falling rate regime by evaporation and diffusion.

1 INTRODUCTION

Recently there has been a major development in the injection molding process for ceramic parts as the need for near-net-shape technology has increased.[1–3] Ceramic injection molding usually includes the following steps: mixing of ceramic powder with the binder system, shaping, debinding, and sintering.[4–6] The binder system in injection molding, which accounts for 40–60 vol% of the mixture, consists of major binder, minor binder, and various processing aids such as surface modifier and plasticizer.[7,8] Since the binder system mainly determines the mixing characteristics and the shaping ability of the mixture,[9–12] the selection of an appropriate binder system is critical for the success of the injection molding process. Usually, the major binder, which controls the general properties of the mixture and green bodies, is selected first. Typically thermoplastic polymers are used in high pressure injection molding, whereas in low pressure injection molding, where the injection pressure is less than 1 MPa, various waxes are most commonly used as the major binder.[3,13]

The binder system used for the shaping should be removed in the debinding step, in which various binder removal techniques can be employed, depending on the type of major binder. When a polymer with a high melting point is used as the major binder, thermal and/or oxidative degradation is usually employed.[14–16] In conventional high pressure injection molding, the minor binder normally has a lower melting point than that of the major one. Thus, the minor binder is eliminated first, leaving continuous pore channels through which the major binder can be readily removed by thermal degradation.[17,18] On the other hand, in low pressure injection molding in which organic materials with low melting points such as wax and oil are used as the major binder, the major binder is debinded first by wicking or solvent extraction and the remaining major binder and the minor binder are removed by thermal and/or oxidative degradation. The minor binder plays an important role in retaining the shape and strength of injection molded bodies during the debinding process.

Regardless of the exact process employed, green bodies are the most vulnerable to the defect formation during debinding, mainly because a large

amount of binder system should be removed and the binder system experiences phase transition of solid to vapor and/or solid to liquid. Since an extremely slow rate of debinding is usually employed to prevent defect generation, the debinding step consumes most of the processing time of injection molding.[19–21] In the practical sense, therefore, it is important to determine the optimum debinding rate for a given binder system. However, fundamentally it is more important to understand the kinetics of debinding so that the causes of the defect formation are apprehended and modifications of the binder system or process can be made.

In the present study, the kinetics of both wicking and solvent extraction were investigated for green compacts containing wax as the major binder. In solvent extraction the controlling step was usually the interdiffusion of binder and solvent, although it could be dissolution of the binder or removal of the dissolved binder at the surface of the sample. When the debinding rate is determined by interdiffusion, the weight fraction of the major binder removed, W, changes parabolically with debinding time as formulated in the following equation for small diffusivity and short time:[22]

$$W = 2(Dt/\pi L^2)^{1/2} \quad (1)$$

Here, D is interdiffusion diffusivity, t is the debinding time, and L is the half-thickness of the green bodies. The rate of removal, dW/dt, is inversely proportional to the removed amount W:

$$dW/dt = A/W \quad (2)$$

where A is a constant.

The wicking kinetics for permeation-controlled cases have also been formulated in previous studies, for example by German[23] and by Wright and Evans.[24] Although the details of the formulations were different, both models resulted in parabolic relationships between the amount of major binder removed and the wicking time. As for the rate of removal, they also predicted the same equation as shown in eqn (2). However, several unrealistic assumptions were used in these models, resulting in an over-simplification of the actual wicking process. For example, a unidirectional flow of major binder to the powder bed maintaining the planar front was assumed in the models.[22,23] Thus, it ignored the fact that the fluid during the wicking process experiences three stages, which are capillary, funicular, and pendular stages. More importantly, there was no provision in these models for the redistribution of the major binder during the wicking process, in which the fluid moved from coarser to finer pore channels by the difference in capillary pressure. The redistribution of the fluid, which makes the saturation of the green bodies uniform, has also been observed in the thermal degradation process, where the binder system contains a fluid component.[25,26] Although these phenomena have not been reflected in the kinetic equations formulated up to now, Bao and Evans[27,28] pointed out that the wicking process took place in three stages.

The objective of the present study is to investigate the debinding kinetics of both wicking and solvent extraction using either compression molded or injection molded ceramic samples. The variation of pore structure with the progress of debinding will be determined to reveal that green bodies experience different microstructural evolution during wicking and solvent extraction. It will also be shown that wicking is a more complicated process than previously proposed models have suggested.

2 EXPERIMENTAL METHODS

2.1 Materials and preparation of green bodies

The ceramic powder used in this study was a commercial silicon nitride and the binder system consisted of paraffin wax, polyethylene wax and stearic acid. The role and properties of each component, as well as the composition of the mixture, are summarized in Table 1.

The silicon nitride powder and the binder system were mixed as follows. The silicon nitride powder was first coated with the stearic acid by adding the powder to an ethanol solution of stearic acid at 50°C, then ethanol was removed by evaporation. The coated silicon nitride powder was then mixed sequentially with polyethylene wax at 100°C and with paraffin wax at 70°C, both dissolved in toluene.

The samples for measuring the debinding kinetics were formed by compression molding the mixture at 40°C under a pressure of 150 MPa. The compression molded samples were rectangular bars with dimensions of 35 × 8 × 3·5 mm. Ceramic valves were also molded using a low pressure injection molding machine (MIGL-28, Peltsman Co., USA). The mixture was injected into the mold cavity under a pressure of 0·3 MPa and a holding pressure of 0·15 MPa was applied for 20 s. These valves were used to observe both defect formation and binder distribution during the debinding.

2.2 Solvent extraction

Solvent extraction was performed at 50°C using *n*-butanol as the solvent. At this temperature, the

Table 1. Composition of the mixtures and their properties

Component		Source	Properties	Composition (wt%) Compression molded sample	Injection molded sample
Si_3N_4	Ceramic powder	Ube, E10	Average particle size : 0·5 μm	77·6	74
Paraffin wax	Major binder	Dongnam Petroleum, DP-135	Melting point: 56–58°C	12·5	16·9
Polyethylene wax	Minor binder	Lion Chem., L-C 102N	Melting point :107°C	5·7	5·4
Stearic acid	Surfactant	Aldrich, 95%	Melting point 67–69°C	3·9	3·7

solubility of paraffin wax in *n*-butanol[29] is ~17 g/cm^3, while that of polyethylene wax is negligible. This difference in solubility justifies the selection of the solvent.

Bar samples were placed at the center of a beaker which contained ~200 cm^3 of *n*-butanol at 50°C. The solvent was stirred during debinding to remove the dissolved wax quickly from the surface of the sample. The debinded sample, after a pre-determined interval, was vacuum-dried at 40°C to evaporate the solvent, and its weight was measured.

2.3 Wicking debinding

For wicking debinding, the bar samples, embedded in fine alumina powder, were put at the center of a 200 cm^3 alumina crucible. The alumina powder (AKP 30, Sumitomo, Japan) used as the powder bed had an average particle size of 0·35 μm. The whole assembly was tapped until the fractional density of the powder bed reached 28%, and was put in an electrical furnace at 150°C. The variation of sample weight with time was measured.

2.4 Characterization of debinded bodies

The pore size distributions of both the partially and completely debinded samples were measured with a mercury porosimeter (Poresizer 9320, Mocromeritics, USA). To prepare the completely debinded sample, either the wicked or solvent extracted body was further debinded by the thermal degradation up to 600°C. The heating rate to 600°C was 1°C/min, and holding periods were employed at 250°C, 350°C, and 450°C for 5 h at each temperature. The resulting pore size distributions were presented on a volume basis, $D_v(r)$, which could be defined by the following equation:

$$D_v(r) = P/r(\mathrm{d}V/\mathrm{d}P) \quad (3)$$

Here, r is the pore size, and V is the volume intruded by mercury at pressure P.

The distribution of the remaining binder within the partially debinded bodies was examined by using DSC (PLDSC, PL, England). About 45% of the major binder was removed from the valve stem by both solvent extraction and wicking, following the aforementioned procedures. The variations of the DSC peaks were observed for the peripheral and central regions of the debinded stems for both samples.

3 RESULTS

Figures 1(a) and (b) show the variation of weight loss with debinding time for solvent extraction and wicking, respectively. The percentage of weight loss was determined with respect to the amount of major binder, e.g. paraffin wax. In doing so, the solubility of polyethylene wax in paraffin wax was neglected, since the mutual solubility, if any, does not appear to have a significant effect on debinding characteristics such as pore structure evolution and binder distribution, etc. When the percentage of weight loss was plotted against $t^{1/2}$, most of the data for the solvent extraction fell on a straight line with a constant slope as shown in Fig. 2(a), indicating that the curve in Fig. 1(a) was indeed a parabolic one.[24,27,28] However, when the data for wicking were plotted against $t^{1/2}$, the result could not be represented as a straight line, as shown in Fig. 2(b). In fact, the curve seemed to consist of several segments with different slopes.

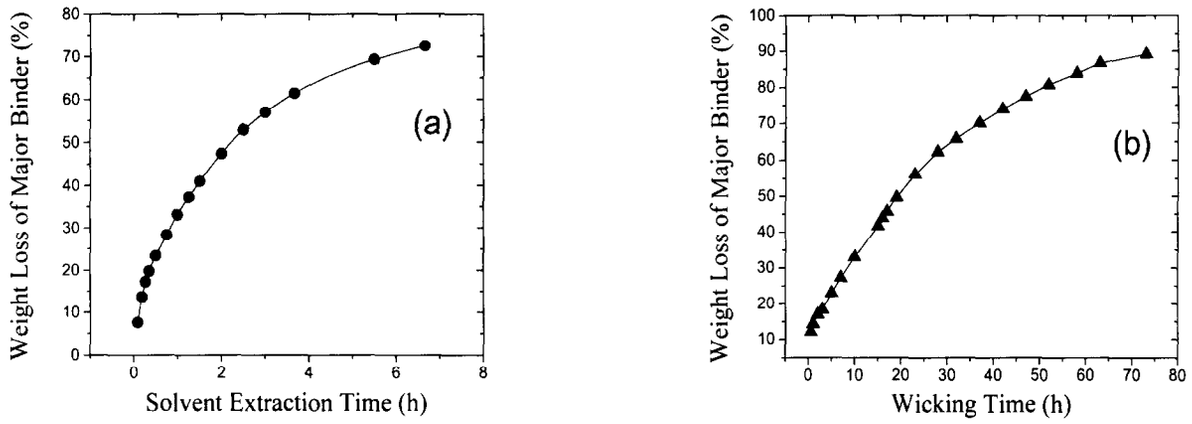

Fig. 1. Percent weight loss as a function of time during (a) solvent extraction and (b) wicking.

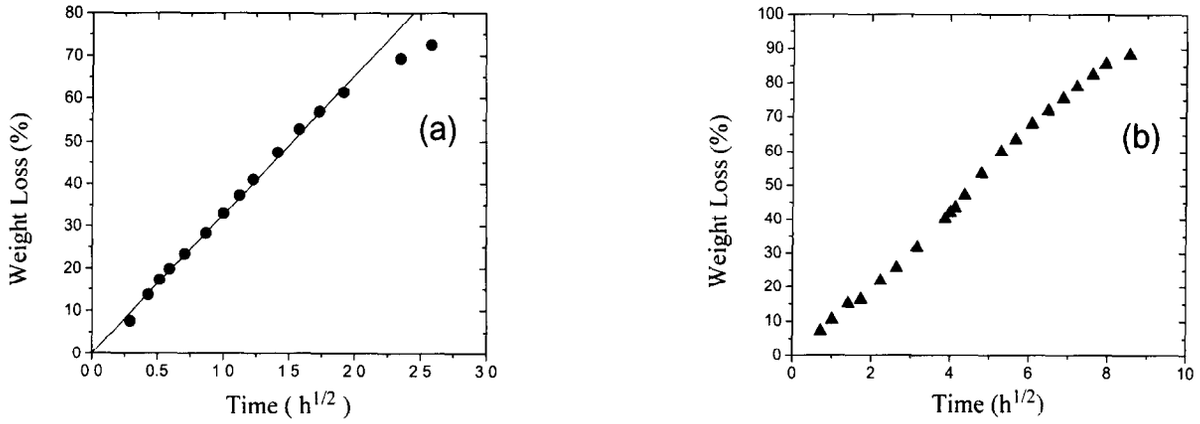

Fig. 2. Percent weight loss vs square root time during (a) solvent extraction and (b) wicking.

This difference between the solvent extraction and the wicking kinetics can be seen more clearly when the rate of weight loss is plotted as a function of weight loss, as shown in Fig. 3. The curve in Fig. 3(a) for the solvent extraction shows that the extraction rate decreases rather smoothly with the amount of extraction. The dotted lines are solvent extraction rates calculated by eqn (1), with diffusivity in the range 10^{-5}–10^{-7} cm^2/s. It is evident from Fig. 3(a) that the diffusivity is about 10^{-6} cm^2/s, which appears reasonable from the literature[18] and the estimation from the slope in Fig. 2(a). The data for wicking shown in Fig. 3(b) demonstrated that the process mainly consisted of four different regimes, not one as in the solvent extraction. In the first regime the wicking rate decreased rapidly up to ~18% weight loss of major binder. Then, there was a regime in which the wicking rate was constant, which extended up to ~46% weight loss of major binder. This second regime was followed by two consecutive regimes with decreasing wicking rate, in which a distinctive change in slope was found at ~67% weight loss of major binder. The decrease of the wicking

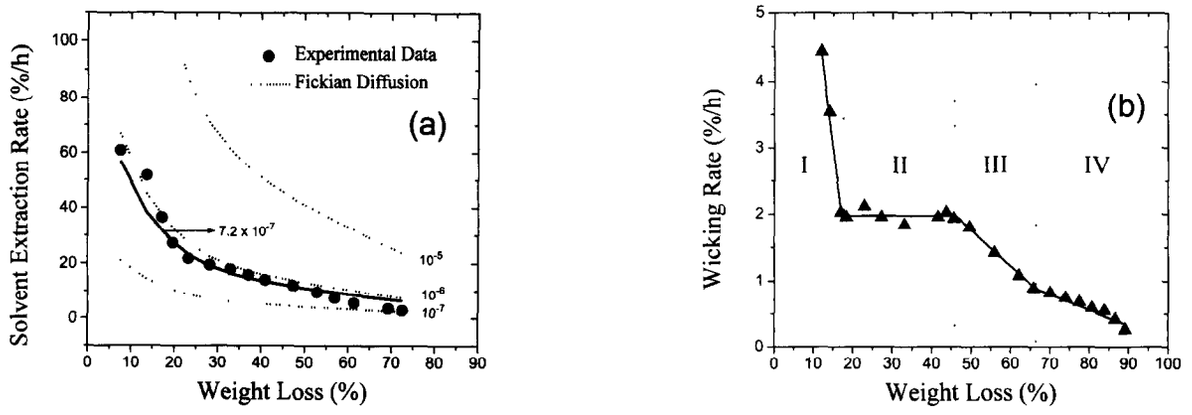

Fig. 3. Debinding rate as a function of percent weight loss during (a) solvent extraction and (b) wicking.

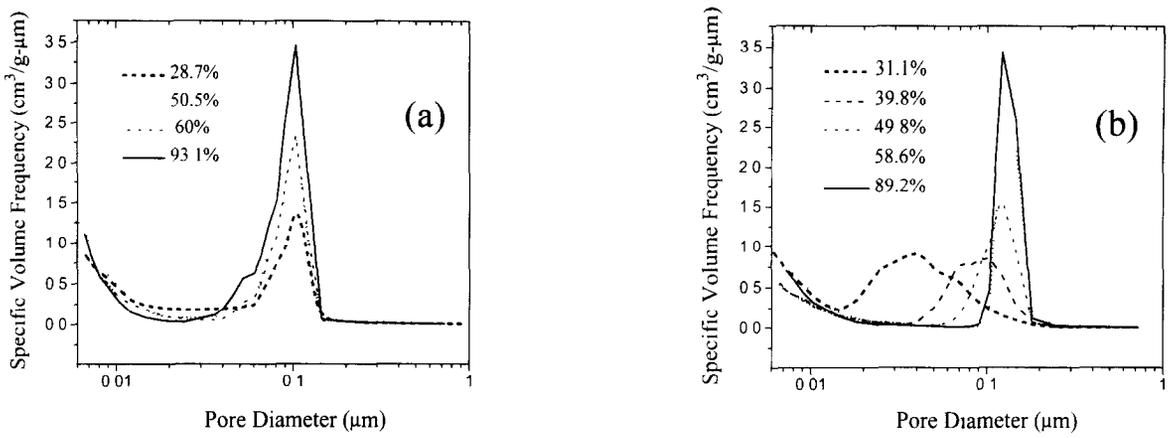

Fig. 4. Pore size distributions of partially debinded samples prepared by (a) solvent extraction and (b) wicking.

rate was moderate in the third regime, while that in the fourth regime was very slow.

In order to correlate the debinding kinetics observed with the microstructural change, the pore size distributions of partially debinded bodies were measured using mercury porosimeter. As shown in Fig. 4(a), the general shape of the pore size distribution curve and size range of pores did not change during solvent extraction except that the volume frequencies for the given pore size range increased with weight loss. On the other hand, Fig. 4(b) shows that the median pore size increased and pore size distribution became narrower with the progress of wicking. The median pore size during wicking increased initially with weight loss, then did not change for a weight loss of ~50% and greater (Fig. 5).

The differences in the debinding behavior between the solvent extraction and wicking processes could be found not only in their pore size distributions but in the distribution of the major binder inside the debinded bodies, as shown in Fig. 6. The two DSC peaks located at 54–60°C and 90–98°C correspond to the melting of paraffin wax and polyethylene wax, respectively. From Fig. 6(a) it is evident that there is a substantial difference in melting temperature, as well as in specific heat of the first peak between near surface and central portions of the sample, which is partially debinded by solvent extraction. Both effects could be attributed to the spatially preferential removal of paraffin wax during solvent extraction. The shift of the melting point to ~61°C at the near surface portion also suggests that stearic acid has considerable solubility in paraffin wax. On the other hand, the DSC results were essentially identical between near surface and central portions in the wicked sample. This indicates that the composition and amount of residual binder are relatively homogeneous throughout the sample partially debinded by wicking,[24,27,28] Therefore, it is believed that the binder could be readily re-distributed during wicking due to the rapid binder flow through capillaries.

In addition, there was significant surface fragmentation when the injection-molded sample was

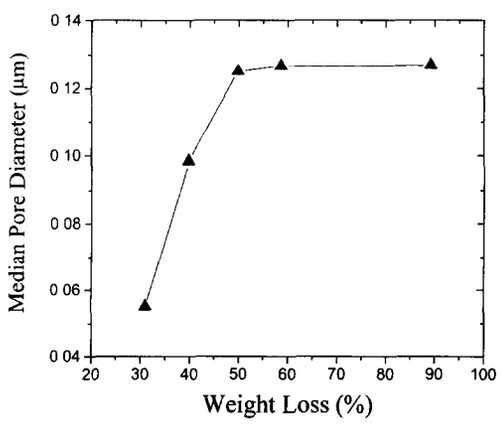

Fig. 5. Variation of median pore diameter as a function of percent weight loss during wicking.

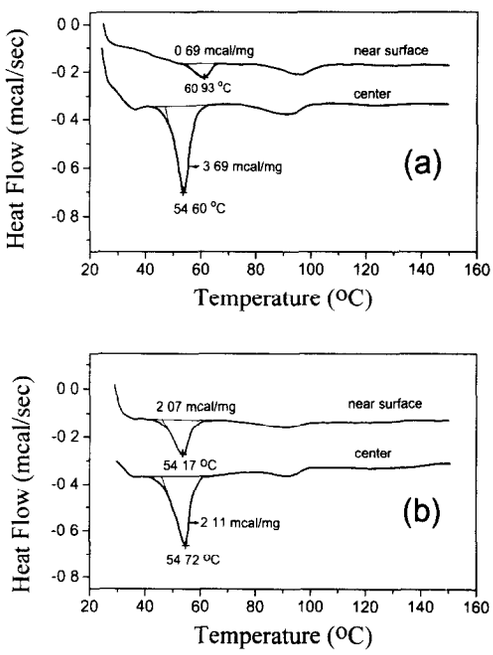

Fig. 6. DSC results obtained from the samples debinded by (a) solvent extraction and (b) wicking.

solvent-extracted. The fragmentation appeared to originate from a lateral crack through the boundary where the capillary structure was discontinuous. That is, the fragmented region is in the pendular state, presumably with the residual minor binder, while the unfragmented central region still remains in the fluid state. Contrary to the injection molded samples, there was no visible defect in the compression-molded samples. This might be attributed to the relatively higher amount of minor binder, as well as increased friction between solid particles in the latter samples.

4 DISCUSSION

The debinding of green bodies is the process in which the volume occupied by the binder system is gradually replaced by the pore. Therefore, the debinding process may be well described by the variation of the degree of saturation, S, which is defined by the ratio of the volume occupied by the binder system to the available pore volume.[30–32] Since the mixtures for compression or injection molding usually contain ceramic powder of less than the critical volume fraction to achieve viscosity low enough for forming, green bodies are in the fluid state ($S > 1$) at the very beginning of debinding. As the excess amount of the binder system is removed, the green bodies reach the capillary state ($S = 1$) in which the volume of the binder system equals available pore volume. After the capillary state, actual pores develop in the green bodies, but the binder system maintains a continuous phase, which is the funicular state ($S < 1$). With further progress of debinding the binder system becomes isolated around the particle and pores form a continuous phase, which corresponds to the pendular state ($S << 1$).

The capillaries containing the binder system in liquid form experience the aforementioned states sequentially during debinding. However, the present results show that the details of the process, such as the pore development and the distribution of the binder system, are dependent on the debinding process employed. In solvent extraction, debinding proceeds from the surface to the center of the sample, with a boundary separating debinded and undebinded regions. The binder system in the debinded region might be completely removed or exists in pendular state near the surface, whereas that in the undebinded central region is still intact, e.g. in fluid state. The presence of the boundary could be directly observed in the partially debinded samples, and the amount of major binder on each side of the boundary, shown in Fig. 6(a), also supports the binder removal process described above. The small amount of the major binder near the surface region might be attributed to either the adsorbed or the condensed layer from the solution.

Since the boundary simply moves inwards with the progress of the debinding by solvent extraction and the packing density is uniform throughout the green bodies, the pore size distribution does not change with the weight loss, as shown in Fig. 4(a). Solvent extraction in the present case is probably diffusion-controlled because the paraffin wax has a relatively high solubility to the solvent used, *n*-butanol, and the dissolved wax is removed continuously by stirring. Evidently, the coincidence of the observed kinetics in Fig. 3(a) with the calculated curve using diffusivity obtained from Fig. 2(a) supports the fact that solvent extraction is indeed a diffusion-controlled process in the present case.

Contrary to solvent extraction, the distribution of the binder system is uniform throughout the green bodies during wicking, as shown in Fig. 6(b), as long as the binder phase is continuous through the capillaries. This is caused by the rapid redistribution of the binder system due to the low viscosity at the wicking temperature. Therefore, debinding proceeds uniformly throughout the green bodies with the help of the rapid redistribution of the binder system, and the capillaries in the green bodies go through the structural changes as a whole. This could be explained by the progressive change of the pore size distributions as shown in Fig. 4(b).

Although the redistribution of the paraffin wax has an important effect on the kinetics of wicking, the wicking process is more complicated, which cannot be explained by the redistribution alone. The first regime in Fig. 3(b) corresponds to the removal of the paraffin wax in a fluid state. The green body is under hydraulic pressure in this regime caused by excess binder system arising from both the excess binder system in the original mixture and much higher thermal expansion of the binder system than that of powder at the wicking temperature.[33] As the hydraulic pressure decreases rapidly with the removal of the paraffin wax, so does the wicking rate. At the end of the first regime the binder system exists in the capillary state.

In the second regime the wicking rate is constant, which has not been observed by other researchers.[23,24,27,28] Although the exact mechanism is not known at present, the constant flow of the paraffin wax per unit time might be possible because of the size difference of capillaries between the green body and the embedding alumina

powder bed. Capillaries in this regime exist presumably in the funicular state. Since the binder system is likely to maintain a continuous channel in this regime, the pores grow gradually throughout the sample with the help of rapid redistribution of binder system as shown in Fig. 4(b) and also in Fig. 5. As the amount of paraffin wax decreases to the level that it cannot maintain a continuous phase in the green bodies, the pendular state begins to appear with isolated binder pockets and the wicking rate starts to decrease. The decrease of the wicking rate in the third regime is, therefore, caused by the transition of capillary structure from funicular to pendular states. When all the pore channels achieve the pendular state at the end of the third regime, debinding by wicking is not possible any longer in the absence of channels for binder flow. In the fourth regime, debinding is thus believed to take place only by evaporation and diffusion.

Once all the capillary structures reached the funicular state in the beginning of the third regime, neither the shape of the pore size distribution (Fig. 4(b)) nor the median pore size (Fig. 5) changed. This reflects that the pore size distribution approached close to the final form with continuous increase of pore volume frequency in this regime, accompanied by the formation of isolated pockets of residual binder in the pendular state. Even in this regime, remaining binder is likely to continue to redistribute itself from coarser to finer pores due to the difference in capillary pressure.[26,34] Figure 7 clearly shows that most of the smaller pores are filled with the binder system, although about 90% of the paraffin wax is debinded from the green body. The size distribution of the pores occupied by the binder system, including the residual paraffin wax, is derived by subtracting the specific volume frequency of the

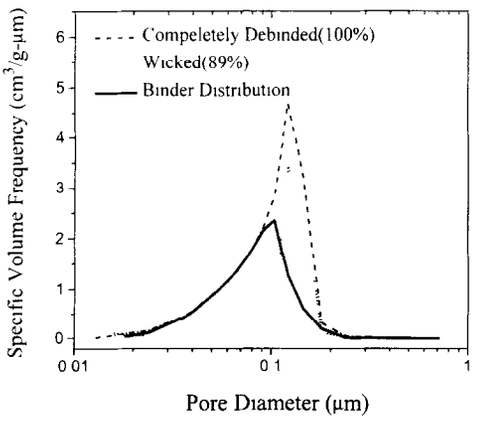

Fig. 7. Capillary size distribution occupied by the remaining binder, obtained by subtracting the specific volume frequency of the 89% wicked sample from that of the completely debinded sample.

green body in the fourth regime from that of the completely debinded body.

The development of pore structures during debinding suggests that the green body debinded by solvent extraction is more vulnerable to defect formation than that debinded by wicking. Since the former has a more non-uniform pore structure than the latter during debinding, stress developed within the green body can cause defect generation. This is more likely when the shape of the green bodies becomes more complex, which explains why the defect is only found in the solvent extracted valve and not in the wicked valve. However, the present result also indicates that defect formation during solvent extraction can be avoided for green bodies with a simple shape by modifying the composition of the binder system. When both the valve stem and compression molded bar samples are debinded by solvent extraction under the same conditions, the debinding defect is found only in the former. Since both samples have rather a simple shape, the result is probably caused by the difference in the binder system (Table 1), especially by the relative amount of minor binder which is responsible for the structural integrity during debinding. Therefore, it is noted that more careful measures should be taken in formulating the binder system for solvent extraction.

5 CONCLUSIONS

The debinding characteristics of plastic-formed samples during both solvent extraction and wicking were investigated using mercury porosimetry and weight loss measurement. The two debinding methods showed significantly different debinding behaviors in kinetics, pore structure evolution, and binder distribution, all of which were correlated. The front of solvent extraction advanced from surface to interior regions with a pendular state left behind, while wicking took place uniformly throughout the sample maintaining a homogeneous distribution of the remaining binder. The solvent extraction rate decayed with a $t^{-1/2}$ dependence, indicating that the process could be described as a diffusion-controlled one. On the other hand, the variation of wicking rate with time was divided into four regimes with three transition points which represented structural changes in capillaries. The first rapidly falling rate regime, corresponding to the transition from fluid to capillary states, was followed by the constant rate regime, corresponding to the transition from capillary to funicular states. Subsequently, the slowly falling rate regime appeared, where the capillary progressively changed from funicular to

pendular states, followed by another falling rate regime during which the debinding took place predominantly by evaporation and gas diffusion through the pore channel.

Both uneven binder distribution and discontinuity in capillary structure across the debinding front during solvent extraction are believed to be the main causes for the observed defects. Therefore, the formulation of the binder system, particularly the type and the amount of the minor binder, is important for successful solvent extraction.

REFERENCES

1. EDIRISINGHE, M. J., Fabrication of engineering ceramics by injection molding. *Am. Ceram. Soc. Bull.*, **70** (1991) 824–8.
2. BANDYOPADHYAY, G. & FRENCH, K. W., Fabrication of near-net-shape silicon nitride parts for engine application. *Trans. ASME.*, **108** (1986) 536–9.
3. MANGLES, J. A., Low-pressure injection molding. *Am. Ceram. Soc. Bull.*, **73** (1994) 37–41.
4. HUNOLD, K., GREIM, J. & LIPP, A., Injection moulded ceramic rotors — Comparison of SiC and Si_3N_4. *Powder Met. Int.*, **21** (1989) 17–23.
5. MANGLES, J. A. & W. TRELA, Ceramic components by injection molding. In *Advances in Ceramics, Vol. 9*, ed. J. Mangles. American Ceramic Society, Columbus, OH, 1984, pp. 220–33.
6. EDIRISINGHE, M. J. & EVANS, J. R. G., Systematic development of the ceramic injection molding process. *Mater. Sci. Eng.*, **A109** (1989) 17–26.
7. GERMAN, R. M., HANS, K. F. & LIN, S. T. P., Key issues in powder injection molding. *Am. Ceram. Soc. Bull.*, **70** (1991) 1294–302.
8. INOUE, M., KIHARA, Y. & ARAKIDA, Y., Injection moulding machine for high-performance ceramics. *Interceram.*, **2** (1989) 53–7.
9. HUNT, K. N. & EVANS, J. R. G., The influence of mixing route on the properties of ceramic injection moulding blends. *Br. Ceram. Trans. J.*, **87** (1988) 17–21.
10. EDIRISINGHE, M. J. & EVANS, J. R. G., Properties of ceramic injection moulding formulations. Part 1: Melt rheology. *J. Mater. Sci.*, **22** (1987) 269–77.
11. STEDMAN, S. J., EVANS, J. R. G. & WOODTHORPE, J., A method for selecting organic materials for ceramic injection moulding. *Ceram. Int.*, **16** (1990) 107–13.
12. EDIRISINGHE, M. J., The effect of processing additives on the properties of a ceramic–polymer formulation. *Ceram. Int.*, **17** (1991) 17–22.
13. KWAK, S. J., KRUG, E. & DANFORTH, S. C., Fracture strength of low-pressure injection-moulded reaction-bonded silicon nitride. *J. Mater. Sci.*, **26** (1991) 3809–12.
14. WOODTHORPE, J., EDIRISINGHE, M. J. & EVANS, J. R. G., Properties of ceramic injection moulding formulation. Part 3: Polymer removal. *Mater. Sci.*, **24** (1989) 1038–48.
15. WRIGHT, J. F., EVANS, J. R. G. & EDIRISINGHE, M. J., Degradation of polyolefin blends used for ceramic injection moulding. *J. Am. Ceram. Soc.*, **72** (1989) 1822–8.
16. JOHNSON, A., CARLSTROM, E., HERMANSSON, L. & CARLSSON, R., Rate-controlled extraction unit for removal of organic binders from injection moulded ceramics. In *Ceramic Powders*, ed. P. Vincenzini. Elsevier Scientific Publishers, Amsterdam, 1983, pp. 767–72.
17. GERMAN, R. M., The thermal debinding of injection molded powder compacts. *Powder Met. Int.*, **22** (1990) 17–22.
18. LIN, S. T. & GERMAN, R. M., Extraction debinding of injection molded parts by condensed solvent. *Powder Met. Int.*, **22** (1989) 19–24.
19. SHAW, H. M., HUTTON, T. J. & EDIRISINGHE, M. J., On the formation of porosity during removal of organic vehicle from injection-moulded ceramic bodies. *J. Mater. Sci. Lett.*, **11** (1992) 1075–7.
20. SHUKLA, V. N. & HILL, D. C., Binder evolution from powder compacts, thermal profile for injection-molded articles. *J. Am. Ceram. Soc.*, **72** (1989) 1797–803.
21. BANDYOPADHYAY, G. & FRENCH, K. W., Effects of powder characteristics on injection molding and burnout cracking. *Am. Ceram. Soc Bull.*, **73** (1994) 107–14.
22. CRANK, J., *The Mathematics of Diffusion*, 2nd edn. Oxford University Press, New York, 1975.
23. GERMAN, R. M., Theory of thermal debinding. *Int J. Powder Mat.*, **23** (1987) 237–45.
24. WRIGHT, J. K. & EVANS, J. R. G., Removal of organic vehicle from moulded ceramic bodies by capillary action. *Ceram. Int.*, **17** (1991) 79–87.
25. CIMA, M. J., DUDZIAK, M. & LEWIS, J. A., Observation of poly[vinyl butyral]–dibutyl phatalate binder capillary migration. *J. Am. Ceram Soc.*, **72** (1989) 1087–90.
26. CIMA, M. J., LEWIS, J. A. & DEVOE, A. D., Binder distribution in ceramic greenware during thermolysis. *J. Am. Ceram. Soc.*, **72**, (1989) 1192–9.
27. BAO, Y. & EVANS, J. R. G., Kinetics of capillary extraction of organic vehicle from ceramic bodies. Part I: Partitioning between porous media. *J. Europ. Ceram. Soc.*, **8** (1991) 81–93.
28. BAO, Y. & EVANS, J. R. G., Kinetics of capillary extraction of organic vehicle from ceramic bodies. Part II: Partitioning between porous media. *J. Europ. Ceram Soc.*, **8** (1991) 95–105.
29. MOZES, G. Y. (ed.), *Paraffin Products: Properties, Technologies, Applications*. Elsevier Scientific Publishers, New York, 1982, p. 124.
30. REED, J. S., *Introduction to the Principles of Ceramic Processing*. John Wiley, New York, 1988, pp. 327–8.
31. SCHERER, G. W., Theory of drying. *J. Am. Ceram. Soc.*, **73** (1990) 3–14.
32. GERMAN, R. M., Powder injection molding. In *Metal Powder Ind. Fed.* Princeton, New Jersey, 1990, pp. 292–301.
33. BARONE, M. R. & ULICNY, J. C., Liquid-phase transport during removal of organic binders in injection-molded ceramics. *J. Am. Ceram. Soc.*, **73** (1990) 3323–33.
34. SHAW, T. M., Liquid redistribution during liquid-phase sintering. *J. Am. Ceram. Soc.*, **69** (1986) 27–34.